catalysts

MDPI

Article

High-Performance A-Site Deficient Perovskite Electrocatalyst for Rechargeable Zn–Air Battery

Chengcheng Wang [1,*], Bingxue Hou [2], Xintao Wang [1], Zhan Yu [1], Dawei Luo [1], Mortaza Gholizadeh [3] and Xincan Fan [1,*]

[1] Shen Zhen Polytechnic, Shenzhen 518055, China; wangxintao@szpt.edu.cn (X.W.); yuzhan198423@szpt.edu.cn (Z.Y.); luodw@szpt.edu.cn (D.L.)
[2] Aviation Engineering Institute, Civil Aviation Flight University of China, Guanghan 618037, China; bingxuehou@foxmail.com
[3] Faculty of Chemical and Petroleum Engineering, University of Tabriz, Tabriz 5166616471, Iran; morteza_gh2000@yahoo.com
* Correspondence: wangchengcheng@szpt.edu.cn (C.W.); horsefxc@szpt.edu.cn (X.F.)

Abstract: Zinc–air batteries are one of the most excellent of the next generation energy devices. However, their application is greatly hampered by the slow kinetics of oxygen reduction reaction (ORR) and oxygen evolution reaction (OER) of air electrode. It is of great importance to develop good oxygen electrocatalysts with long durability as well as low cost. Here, A-site deficient $(SmSr)_{0.95}Co_{0.9}Pt_{0.1}O_3$ perovskites have been studied as potential OER electrocatalysts prepared by EDTA–citrate acid complexing method. OER electrocatalytic performance of $(SmSr)_{0.95}Co_{0.9}Pt_{0.1}O_3$ was also evaluated. $(SmSr)_{0.95}Co_{0.9}Pt_{0.1}O_3$ electrocatalysts exhibited good OER activities in 0.1 M KOH with onset potential and Tafel slope of 1.50 V and 87 mV dec^{-1}, similar to that of $Ba_{0.5}Sr_{0.5}Co_{0.8}Fe_{0.2}O_3$ (BSCF-5582). Assembled rechargeable Zn–air batteries exhibited good discharge potential and charge potential with high stability, respectively. Overall, all results illustrated that $(SmSr)_{0.95}Co_{0.9}Pt_{0.1}O_3$ is an excellent OER electrocatalyst for zinc–air batteries. Additionally, this work opens a good way to synthesize highly efficient electrocatalysts from A-site deficient perovskites.

Keywords: perovskites; oxygen evolution reaction; rechargeable Zn–air battery

Citation: Wang, C.; Hou, B.; Wang, X.; Yu, Z.; Luo, D.; Gholizadeh, M.; Fan, X. High-Performance A-Site Deficient Perovskite Electrocatalyst for Rechargeable Zn–Air Battery. *Catalysts* **2022**, *12*, 703. https://doi.org/10.3390/catal12070703

Academic Editor: Haralampos N. Miras

Received: 20 April 2022
Accepted: 18 June 2022
Published: 27 June 2022

1. Introduction

Rechargeable zinc–air battery has been paid much more attention due to its excellent energy density, safety, and economic costs [1–4]. OER is restricted due to slow kinetics as well as high overpotential [5]. Until now, IrO_2 and RuO_2 have been regarded as efficient commercial OER electrocatalysts. However, the high cost and scarcity greatly restricted the wide commercialization of rechargeable zinc–air batteries [6]. Hence, it is urgent to develop non-platinum substances to replace RuO_2 and IrO_2 electrocatalysts. Among what has been mentioned above, perovskite electrocatalysts have been considered practicable electrocatalysts because of low cost, high electronic conductivity, and electrocatalytic activity [7–12].

Perovskite oxides (ABO_3) are able to show good OER activities because of increasing ionic, electronic conductivities and flexible compositional diversification properties. Suntivich et al. [13] studied ABO_3 electrocatalysts with OER activity and concluded that the increasing OER activity was due to, e.g., orbital of first-row transition metal. $Ba_{0.5}Sr_{0.5}Co_{0.8}Fe_{0.2}O_3$ (BSCF-5582) perovskites [13] have been reported to be highly active catalysts, which could be comparable to IrO_2, however, BSCF-5582 perovskite structure could easily become amorphous after a long-time test. Therefore, a lot of perovskite oxides have been studied as potential OER electrocatalysts, such as $SrNb_{0.1}Co_{0.7}Fe_{0.2}O_{3-\delta}$ [14], $SrCo_{0.9}Ti_{0.1}O_{3-\delta}$ [15], $BaCo_{0.9-x}Fe_xSn_{0.1}O_{3-\delta}$ [16], $La_{0.3}(Ba_{0.5}Sr_{0.5})_{0.7}Co_{0.8}Fe_{0.2}O_3$ [17], and

$SrCo_{0.95}P_{0.05}O_3$ (SCP) [18]. Great efforts could be made to develop perovskite OER catalysts with a good activity as well as stability.

There have been many reports regarding tuning A-site deficient perovskites by yielding positive effects on the electrocatalytic activity toward OER [19–28]. Zhu YL et al. [19] reported that $La_{0.95}FeO_{3\text{-delta}}$ ($L_{0.95}F$) demonstrated the highest OER activity due to surface oxygen vacancies, highlighting the importance of cation deficiency in perovskites by enhancing OER activity. Moreover, Wu XY et al. [20] reported A-site deficient BSCF nanofibers (300 nm diameter) prepared by electrospinning and found OER potential of optimized BSCF, which was stable after long-time tests. It was also reported that it had a great potential in the field of aqueous and flexible zinc–air batteries. However, the universality of deficient effects and mechanisms on ABO_3 perovskite were ambiguous and needed to be clarified.

In this paper, A-site deficient $(SmSr)_{0.95}Co_{0.9}Pt_{0.1}O_3$ perovskites with OER performance under alkaline condition in the application of rechargeable zinc–air batteries were studied in detail. $(SmSr)_{0.95}Co_{0.9}Pt_{0.1}O_3$ delivered good OER activity and stability. Assembled initial Zn–air battery by $(SmSr)_{0.95}Co_{0.9}Pt_{0.1}O_3$ exhibited good cycling stability. This work sheds light on a facile method to prepare $(SmSr)_{0.95}Co_{0.9}Pt_{0.1}O_3$ perovskite electrocatalyst and enhance its potential application of rechargeable zinc–air battery.

2. Results and Discussions

2.1. Phase and Microstructure Characterization

Figure 1 illustrates the XRD patterns of $(SmSr)_{0.95}Co_{0.9}Pt_{0.1}O_3$ sample sintered at 850 °C for 3 h. The sample showed perovskite structure, which was similar to that of published results regarding $Sm_{0.5}Sr_{0.5}CoO_3$. The inverted triangles in the XRD pattern referred to different crystal planes of perovskite structure [29]. ICP-OES test results can indicate that Co was 25.4290 wt%, Pt was 7.2015 wt%, Sm was 22.2669 wt%, Sr was 19.7917 wt%, and O was 25.3109 wt%. Figure 2a shows SEM images of the catalyst for $(SmSr)_{0.95}Co_{0.9}Pt_{0.1}O_3$ sample. Nanoparticles were columnar and the average size was around 150–250 nm. TEM images for $(SmSr)_{0.95}Co_{0.9}Pt_{0.1}O_3$ catalysts are also shown in Figure 2b. The large size was probably due to the sintering and aggregation during heat treatment. As shown in the HADDF images (Figure 3), homogeneity features were found in $(SmSr)_{0.95}Co_{0.9}Pt_{0.1}O_3$, which suggested the distributing of particle sizes in TEM. Sm, Sr, Co, Pt, and O elements were overlapped well and distributed homogeneously within the structure according to the element mapping result. Figure 2c,d demonstrate that the SAED pattern of $(SmSr)_{0.95}Co_{0.9}Pt_{0.1}O_3$ gave Debye–Scherrer rings, confirming the crystalline nature. The d-spacing of 0.297 nm was indexed to the (110) plane of ABO_3 perovskites, as shown in Figure 2c. The selected-area electron diffraction (SAED) pattern of nanoparticles is shown in Figure 2d, imparting a crystalline nature.

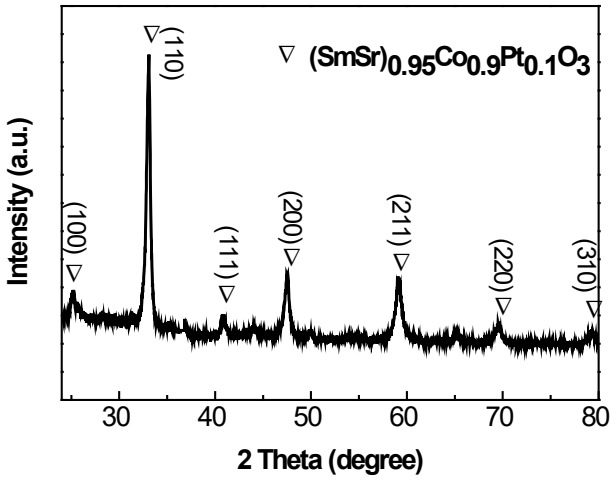

Figure 1. XRD patterns of as-prepared $(SmSr)_{0.95}Co_{0.9}Pt_{0.1}O_3$.

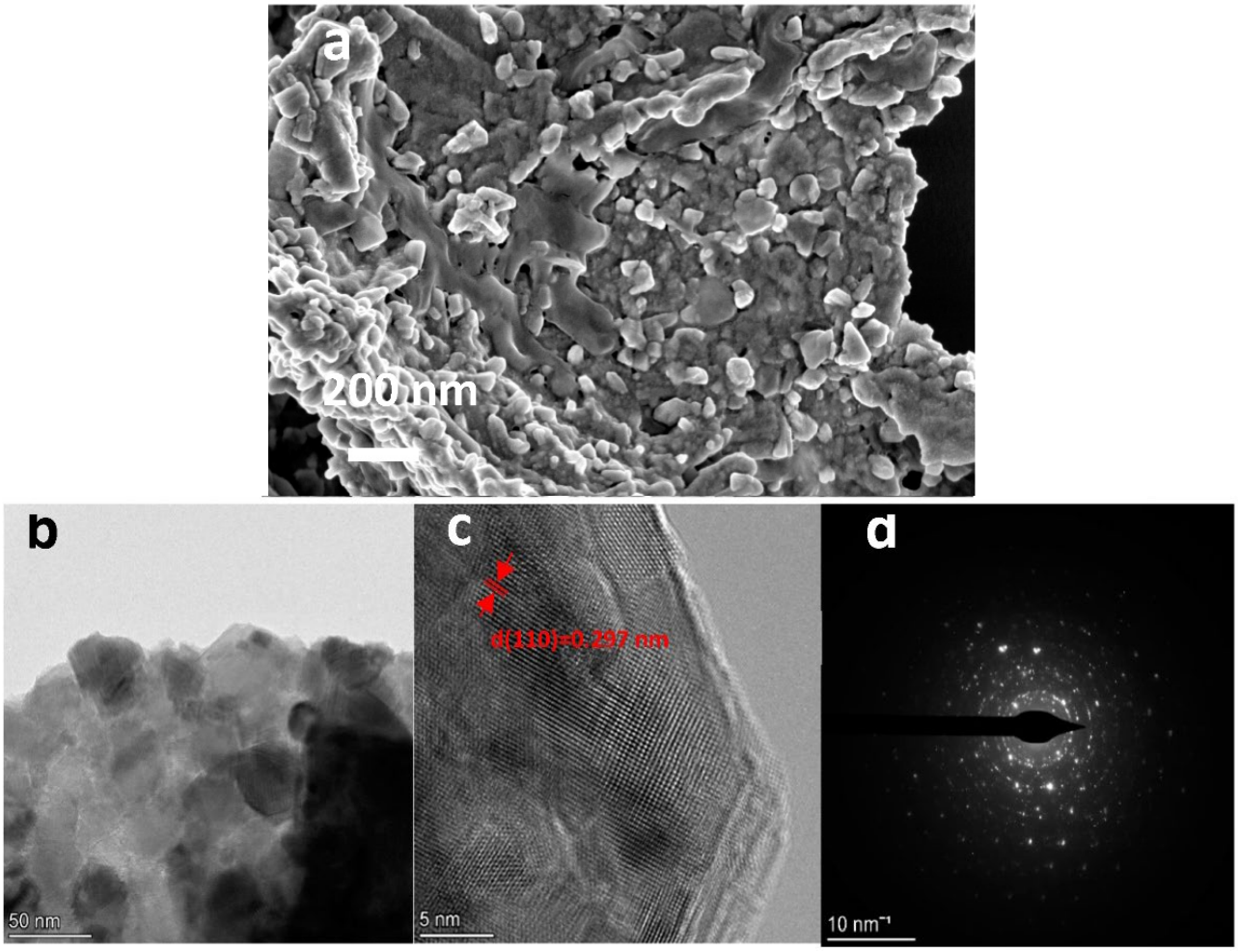

Figure 2. (**a**) SEM image of $(SmSr)_{0.95}Co_{0.9}Pt_{0.1}O_3$. (**b**,**c**) HRTEM images for $(SmSr)_{0.95}Co_{0.9}Pt_{0.1}O_3$. (**d**) Corresponding higher resolution SAED patterns.

The electrocatalytic behavior of perovskites was strongly relied on the valence state of transition metal as well as O anion ordering on catalysts' surface [30–33]. Figure 4a shows the survey scan of the catalysts for $(SmSr)_{0.95}Co_{0.9}Pt_{0.1}O_3$ electrocatalysts, indicating the presence of Sm, Sr, Co, and O elements. Moreover, some unknown elements? were also detected, which might be due to the contamination of tests. Deconvoluted Co 2p and Pt 4f, O1s spectra of the electrocatalyst are shown in Figure 4b,c. Upon deconvolution, $Co2p_{3/2}$ (about 780.0 eV) and $Co2p_{1/2}$ (about 795.2 eV) peaks corresponding to Co^{3+} were observed. Besides, O 1s spectra (Figure 4c) was deconvoluted into two peaks [31]. The first one was a highly oxidative oxygen species (530.4 eV for O_2^{2-}/O^-) and the second one was hydroxyl group or the surface-adsorbed oxygen (531.4 eV for OH^- or O_2) [34]. From what has been mentioned in the paper, good OER activity in an alkaline solution might be attributed to O_2^{2-}/O^- on the surface of catalysts [17,35].

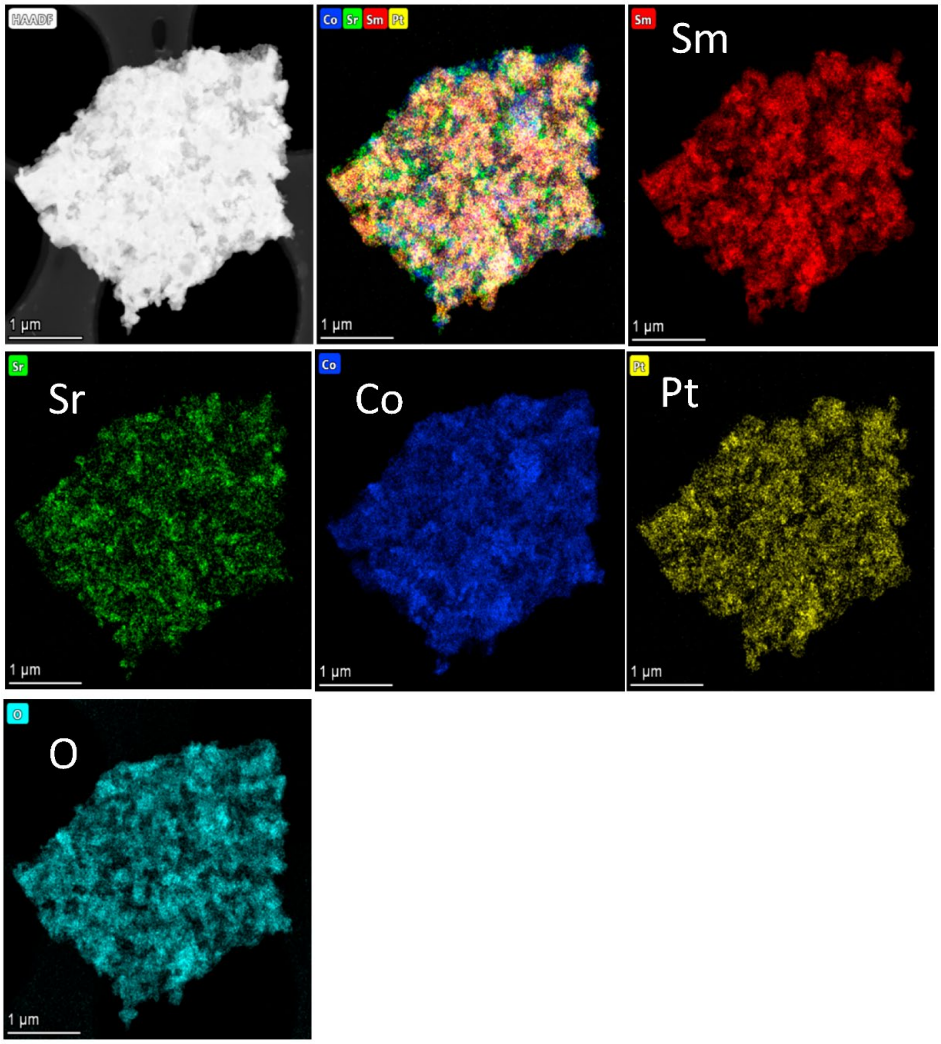

Figure 3. HADDF image and EDS element mappings of Sm, Sr, Co, Pt, and O.

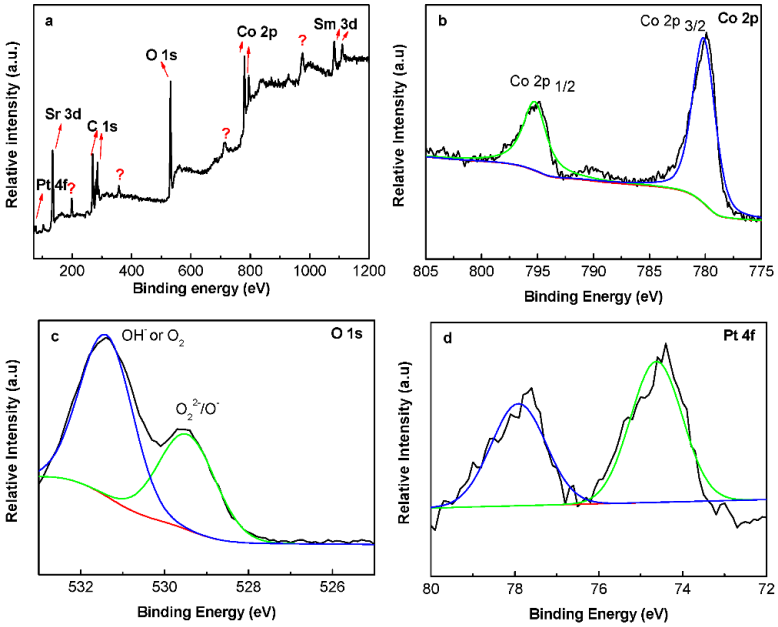

Figure 4. (**a**) Survey scan of $(SmSr)_{0.95}Co_{0.9}Pt_{0.1}O_3$, XPS spectra of (**b**) the deconvolution result of Co 2p. (**c**) The deconvolution result of O 1 s. (**d**) The deconvolution result of Pt 4f.

2.2. Electrocatalytic Performance

Figure 5a shows OER activity of $(SmSr)_{0.95}Co_{0.9}Pt_{0.1}O_3$ electrodes under O_2–0.1 M KOH at 5 mV/s at 1600 rpm. $(SmSr)_{0.95}Co_{0.9}Pt_{0.1}O_3$ showed good OER activity with onset potential of ~1.58 V, which was similar to that of BSCF (1.61 V). The maximum current density measured at 2.0 V was 27 mA cm^{-2} for $(SmSr)_{0.95}Co_{0.9}Pt_{0.1}O_3$, which was similar to that of BSCF (26.7 mA cm^{-2}). Table 1 lists the OER activity of $(SmSr)_{0.95}Co_{0.9}Pt_{0.1}O_3$ with BSCF perovskite-based catalysts in 0.1 M KOH. The results showed its great potential as a highly efficient OER electrocatalyst. Nitrogen adsorption/desorption isotherm patterns of $(SmSr)_{0.95}Co_{0.9}Pt_{0.1}O_3$ and BSCF-5582 are also shown in Figure 6.

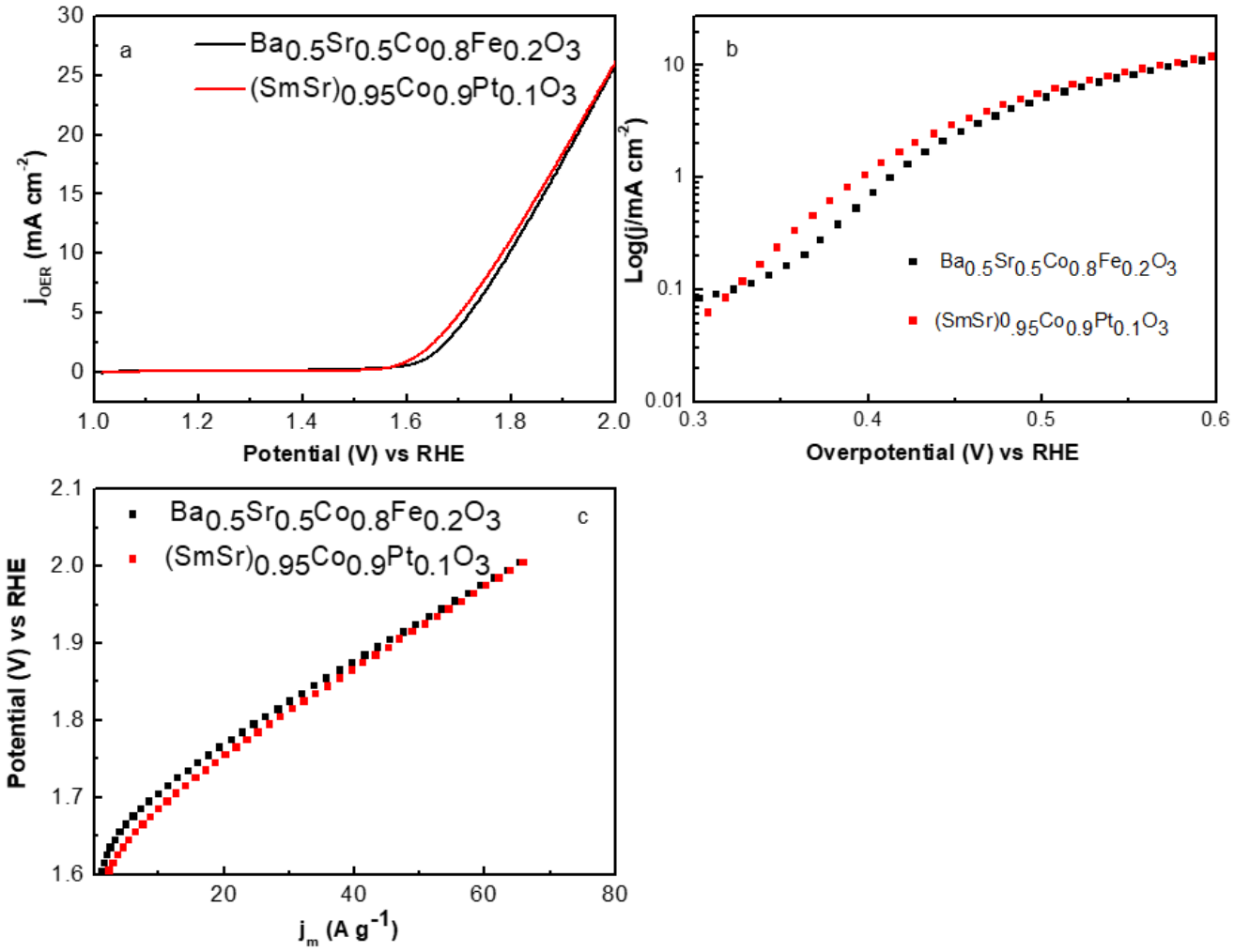

Figure 5. (**a**) LSV curves of $(SmSr)_{0.95}Co_{0.9}Pt_{0.1}O_3$, $Ba_{0.5}S_{r0.5}Co_{0.8}Fe_{0.2}O_3$ catalysts for OER at 5 mV s^{-1} scan rate. (**b**) Tafel plots and corresponding fitted slopes at 1 mV s^{-1}. (**c**) MA comparison.

Table 1. Physical and electrocatalytic properties of the perovskite-based catalyst materials studied in 0.1 M KOH including $Ba_{0.5}S_{r0.5}Co_{0.8}Fe_{0.2}O_3$ and $(SmSr)_{0.95}Co_{0.9}Pt_{0.1}O_3$.

Sample	$Ba_{0.5}Sr_{0.5}Co_{0.8}Fe_{0.2}O_3$	$(SmSr)_{0.95}Co_{0.9}Pt_{0.1}O_3$
BET surface area (m^2 g^{-1})	10.84 ± 0.02	14.77 ± 0.03
ECSA(m^2 g^{-1})	1.79 ± 0.01	1.56 ± 0.02
Onset potential (V)	1.61V	~1.58 V
J_{max} (mA cm^{-2}) (η = 0.77 V)	26.7	27
Tafel slope (mV dec^{-1})	80	82

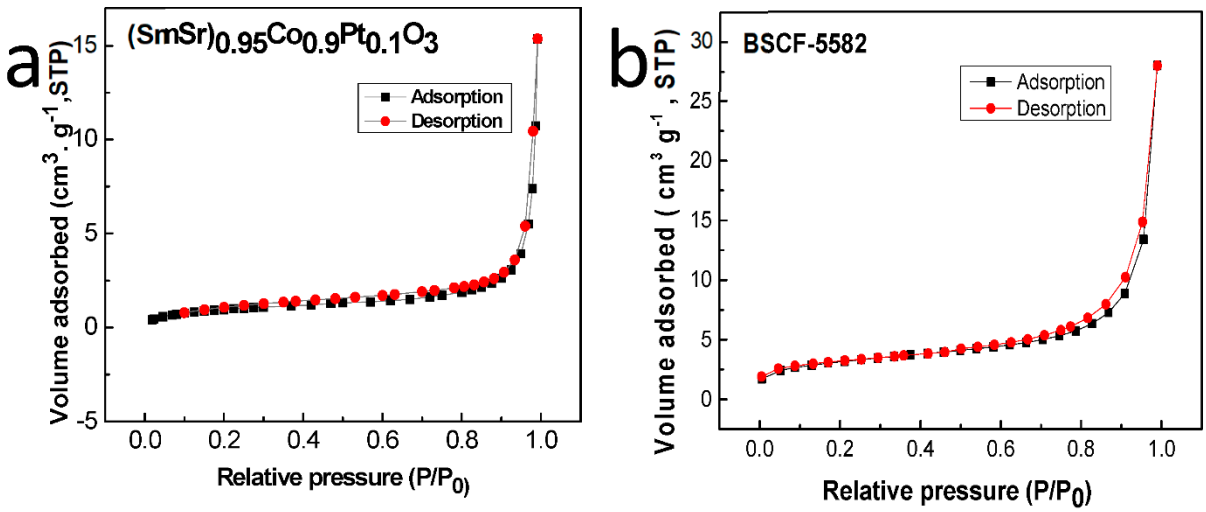

Figure 6. Nitrogen adsorption/desorption isotherm patterns of $(SmSr)_{0.95}Co_{0.9}Pt_{0.1}O_3$ (**a**) and $Ba_{0.5}S_{r0.5}Co_{0.8}Fe_{0.2}O_3$ (BSCF-5582) (**b**).

Figure 5b shows Tafel slope plots for $(SmSr)_{0.95}Co_{0.9}Pt_{0.1}O_3$ and BSCF, measured in 0.1 M KOH solution at 1 mV/s. Tafel slope of $(SmSr)_{0.95}Co_{0.9}Pt_{0.1}O_3$ was 82 mV dec^{-1}, which was similar to that of 80 mV dec^{-1} obtained on BSCF. Zhu et al. reported Tafel slope of 76 and 94 mV dec^{-1} at low overpotentials for $SrNb_{0.1}Co_{0.7}Fe_{0.2}O_3$ and BSCF [14]. Figure 5c further compares the mass activity of $(SmSr)_{0.95}Co_{0.9}Pt_{0.1}O_3$ and BSCF catalysts. Mass activity for $(SmSr)_{0.95}Co_{0.9}Pt_{0.1}O_3$ at (η = 0.77 V) was 66 A g^{-1}, while for BSCF was 65 A g^{-1}. According to the results, the electrochemical activity of $(SmSr)_{0.95}Co_{0.9}Pt_{0.1}O_3$ catalysts was also comparable with that of BSCF. The BET surface area of $(SmSr)_{0.95}Co_{0.9}Pt_{0.1}O_3$ sample is shown in Figure 6. Relatively lower Tafel slope might indicate higher increase of current density, lower overpotential, faster reaction coefficient, which can indicate the relatively higher electrochemical performance.

The electrochemically active surface area (ECSA) of $(SmSr)_{0.95}Co_{0.9}Pt_{0.1}O_3$ and BSCF was calculated from CDL of catalytic surface (a general specific capacitance Cs = 0.040 mF cm^{-2} was used to estimate ESA for carbon proposed by McCrory et al. [36]). Figure 7 shows that based on the slopes, ECSA was 1.79, and 1.56 m^2 g^{-1} for BSCF-5582 and $(SmSr)_{0.95}Co_{0.9}Pt_{0.1}O_3$, respectively. The ECSA of catalysts was smaller than BET surface area.

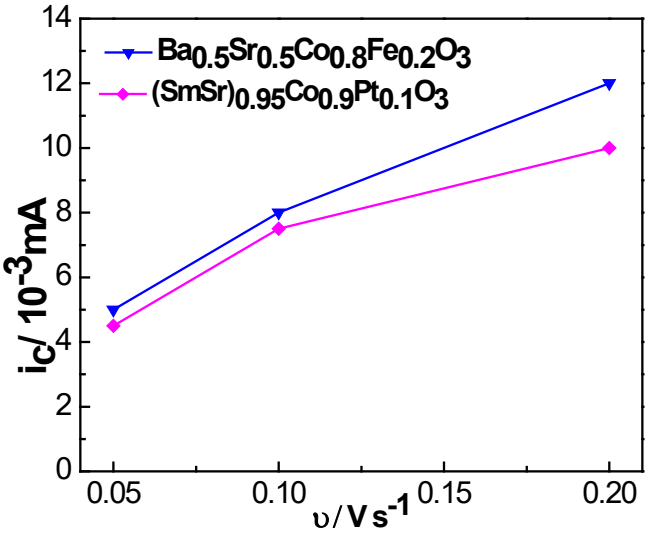

Figure 7. Anodic charging currents measured at 0.01 V plotted as a function of scan rate for $(SmSr)_{0.95}Co_{0.9}Pt_{0.1}O_3$ and $Ba_{0.5}S_{r0.5}Co_{0.8}Fe_{0.2}O_3$ powders in 0.1M KOH solution.

Figure 8a shows chronopotentiometry results at different current densities for BSCF and $(SmSr)_{0.95}Co_{0.9}Pt_{0.1}O_3$ catalysts measured in 0.1 M KOH. Potential to achieve 2, 5, and 10 mA/cm^2 for $(SmSr)_{0.95}Co_{0.9}Pt_{0.1}O_3$, which was fired at 850 °C, was 1.534, 1.568, and 1.590 V, respectively. The potential of BSCF was 1.630, 1.646, and 1.694 V, which was higher than $(SmSr)_{0.95}Co_{0.9}Pt_{0.1}O_3$. The durability of $(SmSr)_{0.95}Co_{0.9}Pt_{0.1}O_3$ fired at 850 °C was studied (Figure 8b), and the potential under 10 mA/cm^2 was 1.605 V, and the potential was around 1.615 V after 10 h. The schematic diagram of $(SmSr)_{0.95}Co_{0.9}Pt_{0.1}O_3$ catalysts for OER in alkaline solution can be seen in Figure 9. Therefore, $(SmSr)_{0.95}Co_{0.9}Pt_{0.1}O_3$ is a good OER catalyst in alkaline condition.

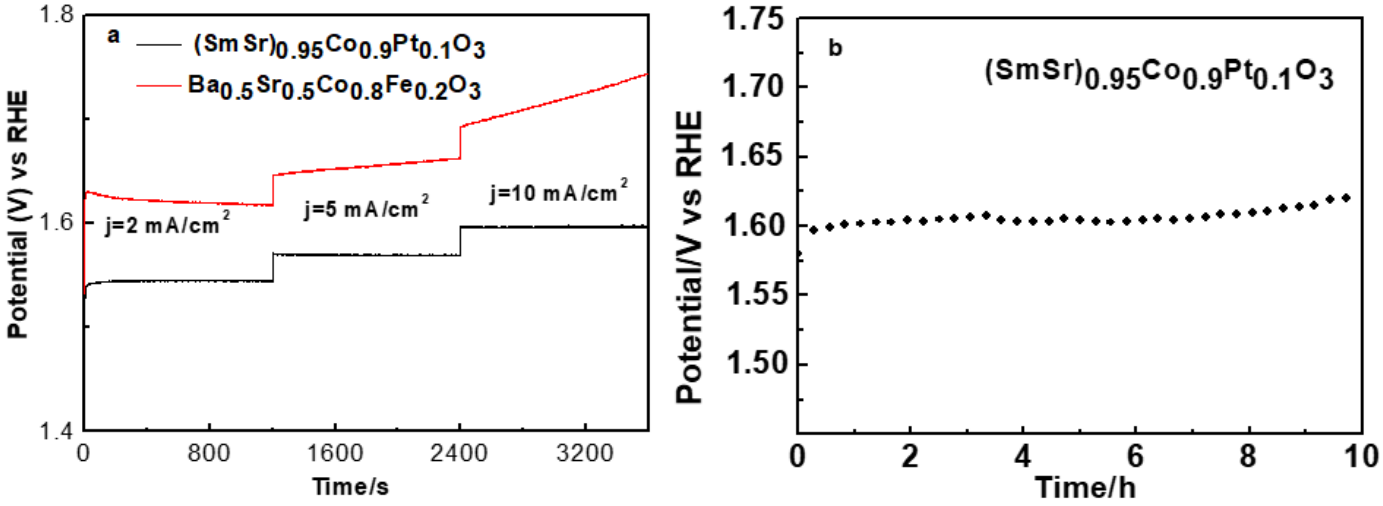

Figure 8. Chronopotentiometry of $(SmSr)_{0.95}Co_{0.9}Pt_{0.1}O_3$ and $Ba_{0.5}S_{r0.5}Co_{0.8}Fe_{0.2}O_3$ (**a**). Stability plots for $(SmSr)_{0.95}Co_{0.9}Pt_{0.1}O_3$ and $Ba_{0.5}S_{r0.5}Co_{0.8}Fe_{0.2}O_3$, measured at different current densities. (**b**) Chronopotentiometry responses at 10 mA cm^{-2} of $(SmSr)_{0.95}Co_{0.9}Pt_{0.1}O_3$. The measurements were carried out in 0.1 M KOH solution and the rotating rate of 1600 rpm. Note: testing time from 0 to 1200 s, current density was 2 mA cm^{-2}; testing time from 1200 to 2400 s, current density was 5 mA cm^{-2}; testing time from 2400 to 3600 s, current density was 10 mA cm^{-2}.

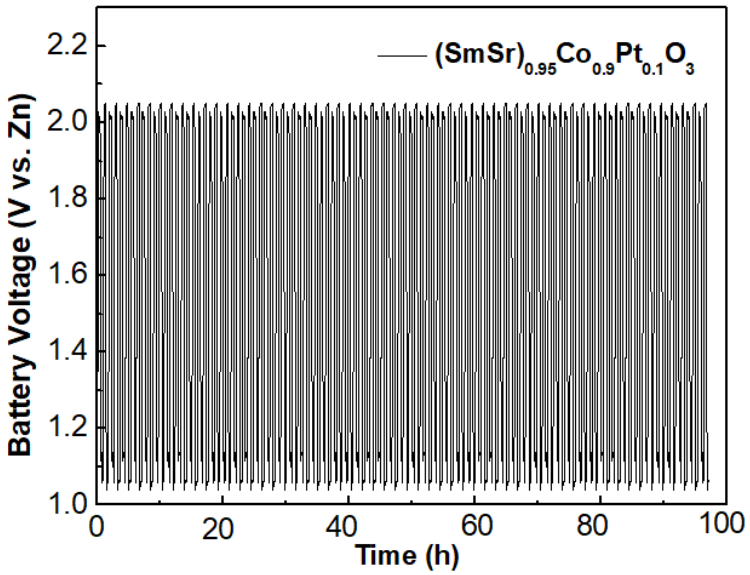

Figure 9. The galvanostatic charge–discharge profiles of rechargeable Zn–air batteries incorporated with catalyst $(SmSr)_{0.95}Co_{0.9}Pt_{0.1}O_3$ mixture at 5 mA cm^{-2}.

2.3. Cell Performance

The practical applicability of $(SmSr)_{0.95}Co_{0.9}Pt_{0.1}O_3$ electrocatalyst was tested in aqueous rechargeable Zn–air battery. Figure 9 shows the stability of Zn–air battery, which was evaluated by charging for 10 min and discharging for 10 min over repeated cycles at 5 mA cm^{-2} for nearly 100 h. Initially, it showed the discharge potential and charge potential of 1.10 V and 2.02V. Therefore, it could be calculated that the voltage gap ($\Delta\eta$) was 0.92 V. After 100 h, voltage gap increased to 1.0 V, respectively. Such a phenomenon was probably due to irreversible Zn plating–stripping process. It can be seen that $(SmSr)_{0.95}Co_{0.9}Pt_{0.1}O_3$-Zn–air battery had potential recharge ability. Moreover, $(SmSr)_{0.95}Co_{0.9}Pt_{0.1}O_3$ is cheaper than commercial IrO_2, which shows its high economic potential.

3. Materials and Methods

3.1. Powder Synthesis

$(SmSr)_{0.95}Co_{0.9}Pt_{0.1}O_3$ powders were synthesized by EDTA–citrate acid complexing method. Stoichiometric mole amounts of $Sm(NO_3)_3{\cdot}6H_2O$, $Sr(NO_3)_2$, $Co(NO_3)_3{\cdot}9H_2O$, and H_2PtClO_4 (CAS: 26023-84-7) were mixed in distilled water with calculated molar ratios of total metal ions/citric acid/EDTA(1:1.5:1). Sol was prepared after mixing and stirring at 80 °C for several hours, and then gel was put into an oven for 12 h at 200 °C to form precursor. Then, the precursor was calcined in air for 3 h at 850 °C. BSCF-5582 powders were prepared as mentioned in our previous paper [37].

3.2. Catalysts Characterization

XRD (Bruker, D8 Advances) was used to test the prepared samples' phase in the range of 5–80° (2θ). N_2 adsorption/desorption isotherms were tested by Micromeritics TriStar II instrument at P/P0 from 0.05 to 0.35. The samples were analyzed by XPS (Thermo Fisher company, ESCALAB 250Xi instrument). SEM from ZEISS was used to characterize the prepared powders' morphology. TEM and EDS were conducted by Titan G2 60–300 microscope.

3.3. Electrochemical Tests

$(SmSr)_{0.95}Co_{0.9}Pt_{0.1}O_3$ (4 mg) was mixed with 1 mL of an ethanol–Nafion mixture (with ethanol:Nafion = 9:1) to form suspension. Pt wire was used as a counter electrode, and Hg/HgO electrode was used as a reference electrode. Suspension (10 μL) was dipped into glassy carbon rotating disk electrode (GC-RDE, 0.196 cm^2, Pine Research Instrumentation, USA). The catalyst loading was 0.2 mg/cm^2. CV measurements [36] were tested as mentioned in the procedure, which was the same as our previous published paper [37]. The flow rate of oxygen supply was 10 mL/min. Before starting the electrochemical test, oxygen was flowed for 30 min to fill the reaction tank with saturated oxygen. CV was conducted at a 5 mV/s between −1 and 1 V for 5 cycles to obtain stable data. LSV was conducted at a 5 mV/s between 0 and 1 V. Tafel plots were tested at 1 mV/s with rotating speed of 1600 rpm. Chronopotentiometry was conducted at different current densities.

3.4. Battery Assembly and Test

Catalyst inks were prepared as mentioned above and then it was distributed uniformly on the carbon cloth with Ni-foam (current collector). Then, carbon cloth (cathode) and polished zinc plate (anode) were assembled in rechargeable Zn air battery by 6M KOH including 0.2 M $ZnCl_2$. Aqueous Zn–air battery tests were carried out by a LAND CT2001A testing device. Charge and discharge data were obtained at 5 mA cm^{-2}.

4. Conclusions

In conclusion, A-site efficient $(SmSr)_{0.95}Co_{0.9}Pt_{0.1}O_3$ oxygen electrocatalysts were successfully prepared by EDTA–citrate complexing sol-gel approach and adopted as a potential OER electrode in Zn–air battery. Optimized $(SmSr)_{0.95}Co_{0.9}Pt_{0.1}O_3$ electrocatalysts showed a higher OER intrinsic activity and durability, which was comparable with that of BSCF.

Moreover, it had a high durability, good rechargeable Zn–air battery discharge performance and high cycle stability, which could be due to the efficient mass transferring and higher active sites. The results clarified a facile way to prepare non-platinum electrocatalysts for energy storage devices.

Author Contributions: C.W.: writing—original draft, B.H.: formal analysis, X.W.: data curation, Z.Y.: methodology, D.L.: validation, M.G.: writing—review and editing, X.F.: funding acquisition, supervision. All authors have read and agreed to the published version of the manuscript.

Funding: The authors also acknowledge 2022 Research Funding of Shenzhen Polytechnic (6022310007K, 6021310004K0), Shenzhen 2022 collaborative innovation technology program international science and technology, Cooperation Project the Science and Technology Innovation Project of Guangdong Provincial Department of Education (2021KTSCX278) and Sichuan science and technology program (2020YJ0501,2022YFH0044).

Data Availability Statement: Not applicable.

Acknowledgments: The authors acknowledge the facilities, scientific and technical assistance from Hoffman Research Institute in Shenzhen Polytechnic.

Conflicts of Interest: The authors declare no conflict of interest.

References

1. Cao, R.; Lee, J.S.; Liu, M.L.; Cho, J. Recent Progress in Non-Precious Catalysts for Metal-Air Batteries. *Adv. Energy Mater.* **2012**, *2*, 816–829. [CrossRef]
2. Li, H.; Ma, L.; Han, C.; Wang, Z.; Liu, Z.; Tang, Z.; Zhi, C. Advanced rechargeable zinc-based batteries: Recent progress and future perspectives. *Nano Energy* **2019**, *62*, 550–587. [CrossRef]
3. Pan, J.; Xu, Y.Y.; Yang, H.; Dong, Z.; Liu, H.; Xia, B.Y. Advanced Architectures and Relatives of Air Electrodes in Zn-Air Batteries. *Adv. Sci.* **2018**, *5*, 1700691–1700721. [CrossRef] [PubMed]
4. Park, J.; Park, M.; Nam, G.; Lee, J.S.; Cho, J. All-Solid-State Cable-Type Flexible Zinc-Air Battery. *Adv. Mater.* **2015**, *27*, 1396. [CrossRef]
5. Shao, M.; Chang, Q.; Dodelet, J.-P.; Chenitz, R. Recent Advances in Electrocatalysts for Oxygen Reduction Reaction. *Chem. Rev.* **2016**, *116*, 3594–3657. [CrossRef]
6. Debe, M.K. Electrocatalyst approaches and challenges for automotive fuel cells. *Nature* **2012**, *486*, 43–51. [CrossRef]
7. Lefèvre, M.; Proietti, E.; Jaouen, F.; Dodelet, J.-P. Iron-Based Catalysts with Improved Oxygen Reduction Activity in Polymer Electrolyte Fuel Cells. *Science* **2009**, *324*, 71–74. [CrossRef]
8. Wu, G.; More, K.L.; Johnston, C.M.; Zelenay, P. High-performance electrocatalysts for oxygen reduction derived from poly-aniline, iron, and cobalt. *Science* **2011**, *332*, 443–447. [CrossRef]
9. Pan, Y.; Liu, S.; Sun, K.; Chen, X.; Wang, B.; Wu, K.; Cao, X.; Cheong, W.C.; Shen, R.; Han, A.; et al. A bimetallic Zn/Fe polyphthalocyanine-derived single-atom FeN4 catalytic site: A superior trifunctional catalyst for overall water splitting and Zn-air batteries. *Angew. Chem. Int. Ed.* **2018**, *130*, 8750–8754. [CrossRef]
10. Chen, Y.; Li, Z.; Zhu, Y.; Sun, D.; Liu, X.; Xu, L.; Tang, Y. Atomic Fe dispersed on Ndoped carbon hollow nanospheres for high-effificiency electrocatalytic oxygen reduction. *Adv. Mater.* **2019**, *31*, 1806312. [CrossRef]
11. Jasinski, R. A New Fuel Cell Cathode Catalyst. *Nature* **1964**, *201*, 1212–1213. [CrossRef]
12. He, W.; Wang, Y.; Jiang, C.; Lu, L. Structural effects of a carbon matrix in non-precious metal O_2-reduction electrocatalysts. *Chem. Soc. Rev.* **2016**, *45*, 2396–2409. [CrossRef]
13. Suntivich, J.; May, K.J.; Gasteiger, H.A.; Goodenough, J.B.; Shao-Horn, Y. A Perovskite Oxide Optimized for Oxygen Evolution Catalysis from Molecular Orbital Principles. *Science* **2011**, *334*, 1383–1385. [CrossRef]
14. Zhu, Y.; Zhou, W.; Chen, Z.G.; Chen, Y.; Su, C.; Tade, M.O.; Shao, Z. $SrNb_{0.1}Co_{0.7}Fe_{0.2}O_3$-delta perovskite as a next-generation electrocatalyst for oxygen evolution in alkaline solution. *Angew. Chem. Int. Ed. Engl.* **2015**, *54*, 3897–3901. [CrossRef]
15. Su, C.; Wang, W.; Chen, Y.; Yang, G.; Xu, X.; Tade, M.O.; Shao, Z. $SrCo_{0.9}Ti_{0.1}O_3$-delta as a New Electrocatalyst for the Oxygen Evolution Reaction in Alkaline Electrolyte with Stable Performance. *ACS Appl. Mater. Interfaces* **2015**, *7*, 17663–17670. [CrossRef]
16. Xu, X.; Su, C.; Zhou, W.; Zhu, Y.; Chen, Y.; Shao, Z. Co-doping Strategy for Developing Perovskite Oxides as Highly Efficient Electrocatalysts for Oxygen Evolution Reaction. *Adv. Sci.* **2016**, *3*, 1500187–1500193. [CrossRef]
17. Jung, J.-I.; Jeong, H.Y.; Lee, J.-S.; Kim, M.G.; Cho, J. A Bifunctional Perovskite Catalyst for Oxygen Reduction and Evolution. *Angew. Chem. Int. Ed.* **2014**, *53*, 4582–4586. [CrossRef]
18. Zhu, Y.; Zhou, W.; Sunarso, J.; Zhong, Y.; Shao, Z. Phosphorus-Doped Perovskite Oxide as Highly Efficient Water Oxidation Elec-trocatalyst in Alkaline Solution. *Adv. Funct. Mater.* **2016**, *26*, 5862–5872. [CrossRef]
19. Bian, J.J.; Li, Z.P.; Li, N.W.; Sun, C.W. Oxygen Deficient $LaMn_{0.75}Co_{0.25}O_3$-Delta Nanofibers as an Efficient Electrocatalyst for Oxygen Evolution Reaction and Zinc-Air Batteries. *Inorg. Chem.* **2019**, *58*, 8208–8214. [CrossRef]

20. Choi, M.J.; Kim, T.L.; Kim, J.K.; Lee, T.H.; Lee, S.A.; Kim, C.; Hong, K.; Bark, C.W.; Ko, K.T.; Jang, H.W. Enhanced Oxygen Evolution Electrocatalysis in Strained a-Site Cation Deficient $LaNiO_3$ Perovskite Thin Films. *Nano Lett.* **2020**, *20*, 8040–8045. [CrossRef]
21. Jiang, Y.L.; Geng, Z.B.; Yuan, L.; Sun, Y.; Cong, Y.G.; Huang, K.K.; Wang, L.; Zhang, W. Nanoscale Architecture of $RuO_2/La_{0.9}Fe_{0.92}Ru_{0.08-x}O_3$-Delta Composite Via Manipulating the Exsolution of Low Ru-Substituted a-Site Deficient Perovskite. *Acs Sustain. Chem. Eng.* **2018**, *6*, 11999–12005. [CrossRef]
22. Ma, J.J.; Geng, Z.B.; Jiang, Y.L.; Hou, X.Y.; Ge, X.; Wang, Z.Z.; Huang, K.K.; Zhang, W.; Feng, S.H. Exsolution Manipulated Local Surface Cobalt/Iron Alloying and Dealloying Conversion in $La_{0.95}Fe_{0.8}Co_{0.2}O_3$ Perovskite for Oxygen Evolution Reaction. *J. Alloy. Compd.* **2021**, *854*, 157154–157161. [CrossRef]
23. Majee, R.; Islam, Q.A.; Mondal, S.; Bhattacharyya, S. An electrochemically reversible lattice with redox active A-sites of double perovskite oxide nanosheets to reinforce oxygen electrocatalysis. *Chem. Sci.* **2020**, *11*, 10180–10189. [CrossRef]
24. Miao, H.; Wu, X.Y.; Chen, B.; Wang, Q.; Wang, F.; Wang, J.T.; Zhang, C.F.; Zhang, H.C.; Yuan, J.L.; Zhang, Q.J. A-Site Deficient/Excessive Effects of $LaMnO_3$ Perovskite as Bifunctional Oxygen Catalyst for Zinc-Air Batteries. *Electrochim. Acta* **2020**, *333*, 135566–135577. [CrossRef]
25. Wu, X.; Miao, H.; Hu, R.; Chen, B.; Yin, M.; Zhang, H.; Xia, L.; Zhang, C.; Yuan, J. A-site deficient perovskite nanofibers boost oxygen evolution reaction for zinc-air batteries. *Appl. Surf. Sci.* **2021**, *536*, 147806–147813. [CrossRef]
26. Xu, W.; Yan, L.; Teich, L.; Liaw, S.; Zhou, M.; Luo, H. Polymer-assisted chemical solution synthesis of $La_{0.8}Sr_{0.2}MnO_3$-based perovskite with A-site deficiency and cobalt-doping for bifunctional oxygen catalyst in alkaline media. *Electrochim. Acta* **2018**, *273*, 80–87. [CrossRef]
27. Yao, X.L.; Liu, J.Y.; Wang, W.H.; Lu, F.; Wang, W.C. Origin of Oer Catalytic Activity Difference of Oxygen-Deficient Perovskites $A_2Mn_2O_5$ (a = Ca, Sr): A Theoretical Study. *J. Chem. Phys.* **2017**, *146*, 1404–1427. [CrossRef]
28. Zhu, Y.; Zhou, W.; Yu, J.; Chen, Y.; Liu, M.; Shao, Z. Enhancing Electrocatalytic Activity of Perovskite Oxides by Tuning Cation Deficiency for Oxygen Reduction and Evolution Reactions. *Chem. Mater.* **2016**, *28*, 1691–1697. [CrossRef]
29. Xia, C.; Rauch, W.; Chen, F.; Liu, M. $Sm_{0.5}Sr_{0.5}CoO_3$ cathodes for low-temperature SOFCs. *Solid State Ion.* **2002**, *148*, A795. [CrossRef]
30. Grimaud, A.; May, K.J.; Carlton, C.E.; Lee, Y.-L.; Risch, M.; Hong, W.T.; Zhou, J.; Shao-Horn, Y. Double perovskites as a family of highly active catalysts for oxygen evolution in alkaline solution. *Nat. Commun.* **2013**, *4*, 2439. [CrossRef] [PubMed]
31. Sun, H.; Chen, G.; Zhu, Y.; Liu, B.; Zhou, W.; Shao, Z. B-Site Cation Ordered Double Perovskites as Efficient and Stable Electrocatalysts for Oxygen Evolution Reaction. *Chem. Eur. J.* **2017**, *23*, 5722–5728. [CrossRef] [PubMed]
32. Gui, L.; Huang, Z.; Li, G.; Wang, Q.; He, B.; Zhao, L. Insights into Ni-Fe couple in perovskite electrocatalysts for highly efficient electrochemical oxygen evolution. *Electrochim. Acta* **2019**, *293*, 240–246. [CrossRef]
33. Zhu, Y.; Zhang, L.; Zhao, B.; Huijun, C.; Liu, X.; Zhao, R.; Wang, X.; Liu, J.; Chen, Y.; Liu, M. Oxygen Defect Engineering: Improving the Activity for Oxygen Evolution Reaction by Tailoring Oxygen Defects in Double Perovskite Oxides. *Adv. Funct. Mater.* **2019**, *29*, 1970236. [CrossRef]
34. Zhu, Y.; Zhou, W.; Chen, Y.; Yu, J.; Liu, M.; Shao, Z. ChemInform Abstract: A High-Performance Electrocatalyst for Oxygen Evolution Reaction: $LiCo_{0.8}Fe_{0.2}O_2$. *ChemInform* **2015**, *47*, 7150–7155. [CrossRef]
35. Liu, R.; Liang, F.; Zhou, W.; Yang, Y.; Zhu, Z. Calcium-doped lanthanum nickelate layered perovskite and nickel oxide nanohybrid for highly efficient water oxidation. *Nano Energy* **2015**, *12*, 115–122. [CrossRef]
36. McCrory, C.C.L.; Jung, S.; Peters, J.C.; Jaramillo, T.F. Benchmarking Heterogeneous Electrocatalysts for the Oxygen Evolution Reaction. *J. Am. Chem. Soc.* **2013**, *135*, 16977–16987. [CrossRef] [PubMed]
37. Wang, C.C.; Cheng, Y.; Ianni, E.; Lin, B. A highly active and stable $La_{0.5}Sr_{0.5}Ni_{0.4}Fe_{0\cdot6}O_3$-δ perovskite electrocatalyst for oxygen evolution reaction in alkaline media. *Electrochim. Acta* **2017**, *246*, 997–1003. [CrossRef]